THE JOURNAL OF PHYSICAL CHEMISTRY C

pubs.acs.org/JPCC Article

Modeling of Diffusion of Acetone in UiO-66

Published as part of The Journal of Physical Chemistry virtual special issue "Carol K. Hall Festschrift".

Jacob J. Wardzala, Jonathan P. Ruffley, Isabella Goodenough, Allie M. Schmidt, Priyanka B. Shukla, Xin Wei, Abhishek Bagusetty, Mattheus De Souza, Prasenjit Das, Dorian J. Thompson, Christopher J. Karwacki, Christopher E. Wilmer, Eric Borguet, Nathaniel L. Rosi, and J. Karl Johnson*

Cite This: *J. Phys. Chem. C* 2020, 124, 28469–28478 Read Online

ACCESS | Metrics & More | Article Recommendations | Supporting Information

ABSTRACT: Highly porous zirconium-based metal–organic frameworks (MOFs) have been widely studied as materials for sorption and destruction of chemical warfare agents (CWAs). It is important to understand the diffusion of CWAs, their reaction products, and environmental molecules through MOFs to utilize these materials for protection against CWA threats. As a first step toward this goal, we study adsorption and diffusion of acetone in pristine UiO-66. We have chosen to study UiO-66 because it has been demonstrated to be effective for destruction of CWAs and simulants; we use acetone because it is a prototypical polar organic molecule small enough to be expected to diffuse fairly rapidly through nondefective UiO-66. We specifically examine the impact of framework flexibility and hydrogen bonding between acetone and the OH groups on the nodes of the framework on the diffusivity of acetone. We find that inclusion of flexibility is essential for meaningful predictions of diffusion of acetone. We have identified the dynamics of the three linkers making up the triangular window between adjacent pores as the critical factor in controlling diffusion of acetone. We demonstrate from experiments and first-principles calculations that acetone readily hydrogen bonds to UiO-66 framework OH groups. We have modified the classical potential for UiO-66 to accurately model the framework–acetone hydrogen bonds, which are not accounted for in many MOF potentials. We find that hydrogen bonding decreases the diffusivity by about 1 order of magnitude at low loading and about a factor of 3 at high loading. Thus, proper accounting of hydrogen bonding and framework flexibility are both critical for obtaining physically realistic values of diffusivities for acetone and similar-sized polar molecules in UiO-66.

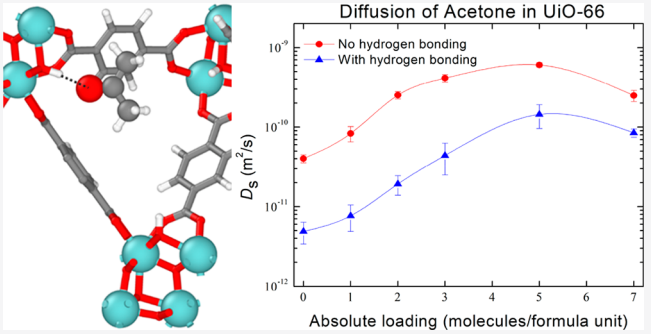

INTRODUCTION

Metal–organic frameworks (MOFs) are porous materials composed of metal oxyhydroxide secondary building units (SBUs) connected by organic ligands (linkers). MOFs have applications in a variety of fields,[1,2] with substantial efforts focused on the use of MOFs for gas separations[3−6] and adsorption.[7−11] MOFs have also been used for chemical warfare agent (CWA) capture and degradation. Specifically, UiO-66 and its derivatives have been widely studied for this purpose.[7,12−16] Effective use of these materials requires an understanding of mass transport limitations because agents must rapidly adsorb and diffuse into the interior of the MOF, where they are temporarily captured (through physisorption) and can react at active sites (through chemisorption at open metal sites) within the MOF.

UiO-66 has a formula unit containing SBUs constructed of 6 Zr atoms with 4 μ_3-O atoms and 4 μ_3-OH groups, coordinated by 12 benzene dicarboxylate (BDC) moieties $[Zr_6(\mu_3\text{-}O)_4(\mu_3\text{-}OH)_4](C_8H_4O_4)_6]$. The μ_3-OH groups may form hydrogen bonds with some CWAs and CWA simulants, which could significantly impact adsorption and diffusion. We note that it has been reported that UiO-66 may be reversibly dehydroxylated by heating to high temperature in a vacuum,[17,18] which eliminates the μ_3-OH groups. We do not consider the dehydroxylated form in this work because under practical conditions UiO-66 would be in its hydroxylated state. The SBUs of UiO-66 are 12 coordinated by BDC linkers, with each linker shared between two SBUs, making all the Zr atoms in the SBU fully coordinated in pristine UiO-66. CWAs are typically too large to diffuse at appreciable rates in pristine UiO-66.[19] In practice, it is defective UiO-66 that is of interest because missing linkers are required for both chemical

Received: July 31, 2020
Revised: December 7, 2020
Published: December 17, 2020

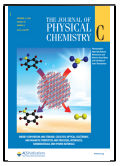

reactivity and enhancing diffusion of CWAs. However, in this work we first seek to understand baseline interactions, adsorption, and diffusion in pristine UiO-66.

Ramsahye and Maurin provide an excellent overview of the calculation of diffusion in MOFs from molecular simulation.[20] Simulation-based methods have been used to study diffusion in MOFs, almost exclusively through the use of classical molecular dynamics.[21−33] However, there is at least one study using density functional theory calculations,[34] but time scales for these simulations are 3 orders of magnitude smaller (tens of picoseconds rather than tens of nanoseconds) than classical potential simulations.

Diffusivities of a variety of molecules in MOFs are reported in the literature, including hydrogen,[23−25,32,34−36] noble gases,[21,22,32] CO_2,[27,30,32] N_2,[27,32] alkanes,[24,27,28,30−32] acetylene,[26] terephthalic acid,[29] benzene,[33] CWAs,[19] and mixtures.[24,25,27,37,38]

An important consideration in simulation studies of diffusion in MOFs is whether to model the framework as rigid or flexible. Many previous simulation studies of diffusion approximated the MOFs framework as being rigid.[21−32] The use of rigid frameworks makes the simulations more computationally efficient and greatly simplifies the construction of the potentials used for simulating the MOFs. Simulations of diffusion using flexible frameworks have also been performed.[22,30,33,34]

Simulations report self-diffusivities[21−34] as well as corrected and transport diffusivities.[21,30,32] We note that these three types of diffusivities are equivalent in the limit of low loading.[39] In this work we report self-diffusion, as calculated from the Einstein relation given by

$$D_S = \frac{1}{2td}\left\langle \sum |r_i(t) - r_i(0)|^2 \right\rangle \quad (1)$$

where t is the time, d is the dimensionality of the system, the sum is over all atoms of diffusing molecules in the system, and the angle brackets denote an ensemble average.

The transport diffusion of benzene, toluene, and xylene through UiO-66 via isothermal diffusion experiments has been studied with in situ infrared (IR) spectroscopy. The pore window was found to limit diffusion, and diffusion rates decreased with increasing molecular size.[40] Diffusion coefficients were on the order of 10^{-10}−10^{-16} m^2/s, and although the guest molecules were nonpolar, IR spectroscopy indicated hydrogen-bonding interactions with the framework μ_3-OH groups. Sharp et al. considered the transport of *n*-butane using in situ IR in UiO-66 and reported diffusion coefficients on the order of 10^{-14} m^2/s.[41]

In this work we seek to elucidate the impact of framework flexibility and hydrogen bonding on adsorption and diffusion of polar molecules in UiO-66. As a first step, we have chosen to study adsorption and diffusion of acetone in pristine UiO-66, reasoning that one should first understand the pristine material before including the impact of missing linker defects, since these defects are difficult to fully characterize. We chose acetone for this study because it is small enough to be expected to diffuse rapidly through the small windows of UiO-66 and also because it is a strongly polar hydrogen bond acceptor but does not self-hydrogen bond. Thus, any hydrogen bonding observed experimentally must be due to acetone−μ_3-OH interactions. We present a combined experimental and theoretical approach to investigate acetone−UiO-66 interactions. We have synthesized and characterized low-defect UiO-66 samples. We have measured μ_3-OH hydrogen bonding in UiO-66 dosed with acetone with FT-IR under ultrahigh-vacuum (UHV) conditions as a function of temperature. We have used molecular simulations to study adsorption and diffusion of acetone in pristine UiO-66.

COMPUTATIONAL METHODS

Molecular dynamics calculations were performed with the Large-scale Atomic/Molecular Massively Parallel Simulator (LAMMPS).[42] Simulations were conducted at zero loading and finite loadings up to saturation vapor pressure and beyond. Zero loading simulations were conducted by turning off interactions between the acetone molecules, thus rigorously excluding any adsorbate−adsorbate interactions. This allowed for simulation of the low loading limit, while obtaining better statistics than simulations having a single molecule in the simulation cell.

A UiO-66 supercell was created that contained 32 formula units (primitive cells). One formula unit contains two tetrahedral pores and one octahedral pore. We used two different flexible force fields for UiO-66, the UFF force field parameters described by Boyd et al.,[43] and the Rogge et al. potential.[44] We used atom-centered charges computed from analysis of our density functional theory (DFT) electron density calculations with the DDEC6 and Chargemol programs[45−48] for both of these potentials. The TraPPE model was used for acetone.[49] A Lennard-Jones model was used for neon.[50] LAMMPS input files containing all the necessary parameters are provided in the Supporting Information. Periodic boundary conditions were applied, and the cutoff was 12.5 Å. A time step of 0.5 fs was used for all simulations. Each run was equilibrated for 50 ps in the canonical (*NVT*) ensemble by using the Nosé−Hoover thermostat.[51,52] Data were collected over 25 ns in the microcanonical (*NVE*) ensemble to avoid artifacts due to the thermostat on the dynamics of the system. Multiple time origins and multiple independent simulations (from 10 to 50) were used to improve statistics.

Acetone in flexible UiO-66 was studied at three temperatures: 325, 350, and 425 K. Each simulation involved 100 noninteracting (i.e., zero loading) acetone molecules inserted into the MOF. Additional simulations were conducted at finite loading using 32, 64, 128, 160, and 224 acetone molecules per simulation cell to model the effect of loading up to saturation. These simulations correspond to 1, 2, 3, 5, and 7 molecules per formula unit, respectively. Saturation loading at 298 K was determined to be close to 6 molecules per formula unit from an adsorption isotherm of acetone by using a methodology we have reported previously.[5,53] Details are given in the Supporting Information, and the isotherm is given in Figure S1. A loading of 7 molecules per formula unit corresponds to an external pressure of acetone beyond the vapor pressure at 298 K (see the Supporting Information). Acetone in rigid UiO-66 was simulated at 325 K. A total of 100 molecules were inserted, and 50 independent runs were used at zero loading.

Simulations of neon in flexible and rigid UiO-66 were conducted at 325 K and contained 500 noninteracting (zero loading) neon atoms. Fifty independent runs were taken for both rigid and flexible models. The mean-squared displacement (MSD) for all molecular dynamics runs was calculated every 100 timesteps for each run by using the center-of-mass formalism. The data were processed as 250 evenly spaced

https://dx.doi.org/10.1021/acs.jpcc.0c07040
J. Phys. Chem. C 2020, 124, 28469−28478

multiple time origins, and diffusion coefficients were calculated via the Einstein relation (eq 1).

Free energy profiles were calculated by using umbrella sampling, as described previously by Agrawal et al.[19] The collective variables (COLVARS)[54] package for LAMMPS was used to implement umbrella sampling. Calculations were performed with 0.1 Å spacing along a reaction coordinate (RC), with a single acetone molecule in the system. The RC was defined as a vector between the centers of a pair of adjacent octahedral and tetrahedral cages, passing through the window that separates the two cages. In each simulation, a harmonic restraint of 41.8 kJ/mol was used to keep the acetone molecule in a region orthogonal to the specified value along the RC. A 50 ps equilibration followed by a 1000 ps production run was performed for each umbrella region. The weighted histogram analysis method (WHAM)[55] was used to combine the independent samples into a free energy profile. These calculations were performed for both forward and reverse barriers, with the forward barrier being defined as the tetrahedral to octahedral cage transition.

DFT calculations were performed to identify the most favorable binding site for acetone in UiO-66. Details are given in the Supporting Information.

EXPERIMENTAL METHODS

We used synthetic conditions reported by Shearer et al.[56] to prepare minimally defective UiO-66 (see the Supporting Information for specific details and characterization of product material).

Temperature-programmed desorption (TPD-MS) and temperature-programmed infrared (TP-IR) measurements were made to characterize the interaction of acetone with UiO-66 in a custom-built ultrahigh-vacuum instrument described in detail previously.[57] Details are given in the Supporting Information.

RESULTS AND DISCUSSION

Adsorption and desorption isotherms of N_2 at 77 K (Figure S5) and acetone at room temperature (Figure S6) were measured experimentally in low-defect UiO-66. Details are reported in the Supporting Information. Grand canonical Monte Carlo (GCMC) simulations were performed to compute isotherms for pristine and defective MOFs (with 4% and 8% missing linkers having defects capped with formate groups) and are plotted along with the experimental data. We find good agreement between simulations and experiments for pristine UiO-66 for N_2 uptake, indicating that the experimentally produced MOFs are close to pristine. In contrast, the simulated acetone isotherm for 8% missing linker defects is in better agreement with experiments than for pristine UiO-66 (details are given in the Supporting Information). The difference between experiments and simulations may be due to inaccuracy of the potential models used or may indicate a higher level of defects than evident from thermogravimetric analysis (Supporting Information).

Plots of the MSD divided by time (MSD/t) as a function of time for acetone in flexible and rigid UiO-66 by using the Boyd et al. potential[43] are shown in Figure 1. Fickian diffusion, described by eq 1, will result in MSD/t being a constant at long times, and this is what is seen for the flexible UiO-66 potential in Figure 1a. In contrast, MSD/t for the rigid model continually and dramatically decreases with time (note the log scale in Figure 1b), indicating that acetone does not diffuse

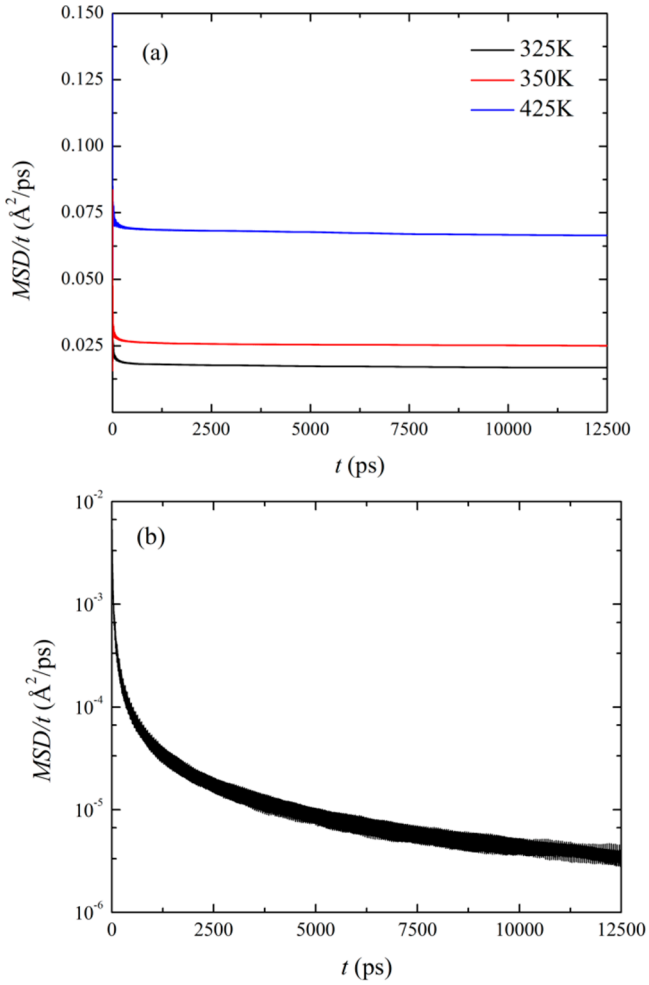

Figure 1. Mean-squared displacement divided by time of acetone in UiO-66 using the (a) flexible or (b) rigid framework model of Boyd et al.[43] at 325 K. Note the semilog scale in (b) required to show exponential decrease in MSD/t with time.

in the rigid model over the time scales of the simulation. We have computed diffusion coefficients for acetone at zero loading as a function of temperature in UiO-66 using three flexible MOF potentials: the Boyd et al. potential,[43] the Rogge et al. potential,[44] and our modification to the Rogge et al. potential, termed TraPPE/Rogge et al., which we describe below. The diffusion coefficients are reported in Table 1 and plotted in Figure 2. The data were fitted to an Arrhenius equation of the form $D = D_0 \exp(-E_A/RT)$ to calculate the diffusion activation energies for these potentials, which are E_A

Table 1. Diffusion Constants of Acetone at Zero Loading in (a) Boyd et al. Flexible UiO-66,[43] (b) Rogge et al. Flexible UiO-66,[44] and (c) TraPPE/Rogge et al. Flexible UiO-66[a]

T (K)	(a) D_s (m²/s)	(b) D_s (m²/s)	(c) D_s (m²/s)
325	$2.80(30) \times 10^{-11}$	$4.02(48) \times 10^{-11}$	$4.88(150) \times 10^{-12}$
350	$4.17(44) \times 10^{-11}$	$6.12(150) \times 10^{-11}$	$9.15(360) \times 10^{-12}$
425	$1.11(62) \times 10^{-10}$	$1.69(30) \times 10^{-10}$	$5.14(140) \times 10^{-11}$

[a]Uncertainties in the least significant digits, given by two standard deviations of the mean, are given in parentheses, e.g., $2.80(30) \times 10^{-11}$ means $2.8 \times 10^{-11} \pm 3.0 \times 10^{-12}$ and $4.88(150) \times 10^{-12}$ means $4.88 \times 10^{-12} \pm 1.5 \times 10^{-12}$.

https://dx.doi.org/10.1021/acs.jpcc.0c07040
J. Phys. Chem. C 2020, 124, 28469−28478

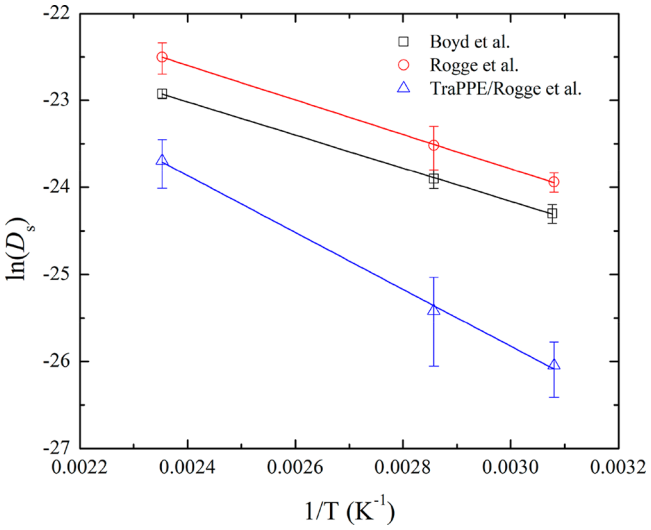

Figure 2. Arrhenius fit of diffusion coefficients for acetone in flexible UiO-66 for three different UiO-66 potentials.

= 15.8, 16.5, and 27.2 kJ/mol for the Boyd et al., Rogge et al., and TraPPE/Rogge et al. potentials, respectively.

To understand the dramatic differences in the MSD for flexible and rigid potentials observed in Figure 1, we have computed the free energy barrier for acetone moving from the center of the tetrahedral pore to the center of the octahedral pore and the reverse path using umbrella sampling combined with WHAM for both the flexible and rigid Boyd et al. UiO-66 potentials. Results for the flexible UiO-66 model, shown in Figure 3a, give a forward (tetrahedral to octahedral pore) barrier of 16 kJ/mol and a reverse barrier of 11 kJ/mol. These barriers are in good agreement with the barrier to diffusion calculated from the Arrhenius equation (Figure 2) of 15.8 kJ/mol. Because the forward barrier is rate-limiting, the effective barrier should be close to the highest barrier. Given this agreement, the Arrhenius equation method was used for the Rogge et al. and TraPPE/Rogge et al. potentials. The free energy minima shown in Figure 3 indicate that the tetrahedral cage is energetically more favorable than the octahedral cage for acetone at low loading. This aligns qualitatively with previous work performed by Agrawal et al.,[19] where it was found that the tetrahedral cage was favored for comparably small molecules while larger molecules favored the more open octahedral cell. Using the rigid model yields an energy profile with a forward barrier of 47.5 kJ/mol and a reverse barrier of 32 kJ/mol, shown in Figure 3b. The dramatic increase in barriers compared to the flexible model explains the failure of the rigid potential to properly exhibit the diffusion of acetone in UiO-66.

To determine whether reasonable diffusion coefficients could be obtained for any molecule by using the rigid UiO-66 model, we considered Ne, which has a kinetic diameter of 0.275 nm,[58] compared with the approximate window size of UiO-66 of about 0.6 nm.[59] One would not expect flexibility to play a measurable role when the diffusing species is significantly smaller than the window size. Surprisingly, we found that Ne diffuses 30% faster in the flexible MOF compared with the rigid model and that this difference is statistically significant. Diffusivities are given in Table 2. Hence, flexibility has an impact on diffusion, even when the window size is much larger than the kinetic diameter of the

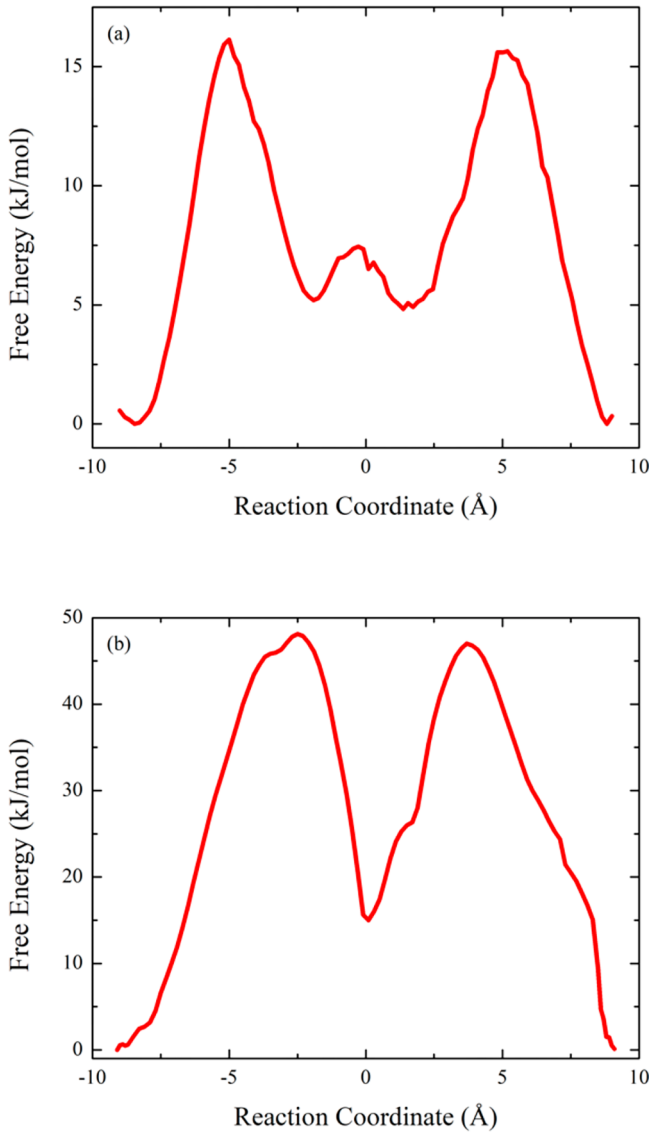

Figure 3. Free energy profiles of acetone traversing the window in the direction from the tetrahedral to the octahedral pore and then from octahedral to tetrahedral (left to right) for UiO-66 with the (a) flexible and (b) rigid Boyd et al.[43] potentials.

Table 2. Diffusivities of Ne in UiO-66 by Using Boyd et al. Flexible and Rigid Framework Models

force field	D_s (m^2/s)
flexible	$2.15(5) \times 10^{-8}$
rigid	$1.44(6) \times 10^{-8}$

diffusing species for UiO-66. This indicates that simulation of diffusion in UiO-66 should use a flexible MOF model to obtain reliable results, especially when the size of the diffusing molecule is close to the size of the pore window. This is in contrast to MOFs such as NU-1000, where a rigid model has produced reasonable diffusion coefficients due to large pore size and channels present in the MOF.[31] The diffusion mechanism of light alkanes has been reported as intercage jumps in UiO-66,[30,60] and that behavior is expected for this system as well. These results, taken together, indicate that ligand flexibility plays a significant role in the movement of molecules through pore windows in UiO-66.

https://dx.doi.org/10.1021/acs.jpcc.0c07040
J. Phys. Chem. C 2020, 124, 28469−28478

We have investigated the molecular-level mechanism of how framework flexibility impacts the diffusivity of acetone by measuring distances between pairs of specific carbon atoms on the benzene rings of adjacent BDC linkers making up the triangular window between the pores of UiO-66 during the process of acetone traversing the pore window. Movies showing the transit of acetone through the window from umbrella sampling simulations are given in the Supporting Information. Plots of the distance between atoms on adjacent pairs of linkers are given in Figure 4. The BDC linkers are

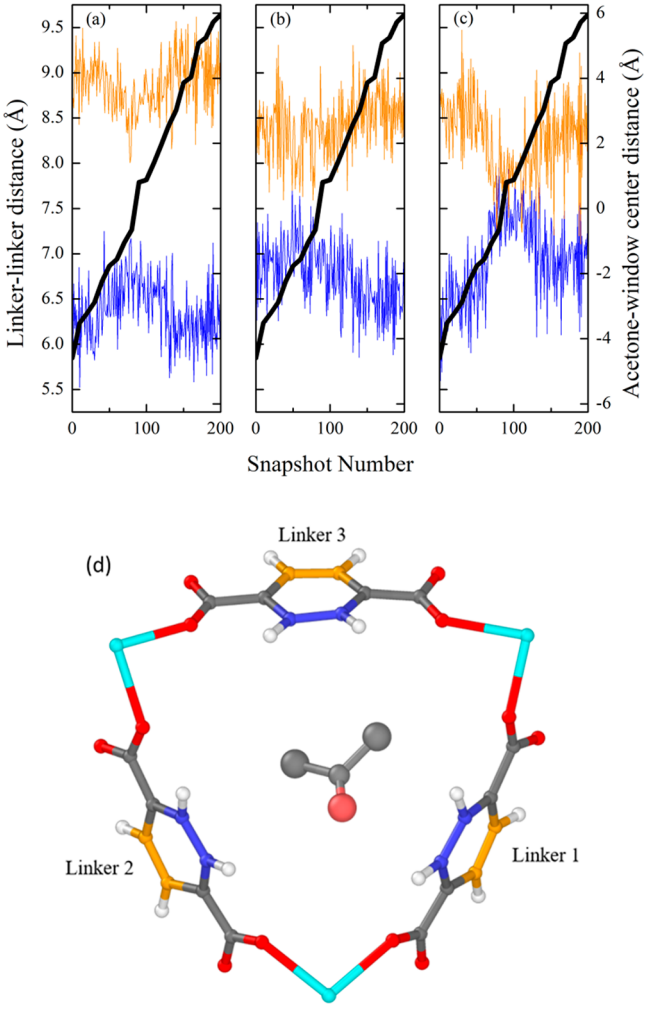

Figure 4. Distances between pairs of carbon atoms making up the window linkers as a function of time (snapshot) for acetone in transit from the tetrahedral to the octahedral pore. The blue lines are for the side of the rings facing the octahedral pore, and the orange lines are for the tetrahedral pore facing side of the rings. Distances shown between (a) linkers 1 and 2, (b) linkers 1 and 3, and (c) linkers 2 and 3, with linkers identified in (d). The black line (right axis) is the distance from the acetone center of mass to the center of the transition window. Movies of the transit are provided in the Supporting Information.

roughly oriented so that one side of the ring is oriented toward the octahedral cage (blue lines) and one is pointing toward the tetrahedral cage (orange lines). Also shown in Figure 4 is the distance of the center of mass of the acetone molecule from the center of the window along the tetrahedral to octahedral path. We see from Figure 4 that the orientation of the linkers dynamically responds as the acetone moves through the window. We note that the acetone molecule does not go through the exact middle of the window but is sometimes closer to one pair of linkers than the others during the transit. The plots show that the linkers open and close to allow acetone to move through the window with a lower barrier. We note that each linker is part of four different windows so that when a pair of linkers "open" to allow a molecule to traverse the window, the windows to other pores are "closed". Hence, it is impossible to orient the linkers such that they are "open" for all pores to which they belong. Plots of the distances between adjacent linkers, similar to the plots in Figure 4, but in the absence of acetone, are presented in Figure S7. Comparison of Figure 4 and Figure S7 shows that the dynamic response of the linkers to the presence of acetone is dramatic.

We next turn to the impact of finite loading on the diffusivity of acetone. We have computed the diffusivity as a function of loading for both the Boyd et al. and Rogge et al. potentials, as shown in Figure 5. We see qualitative agreement between these

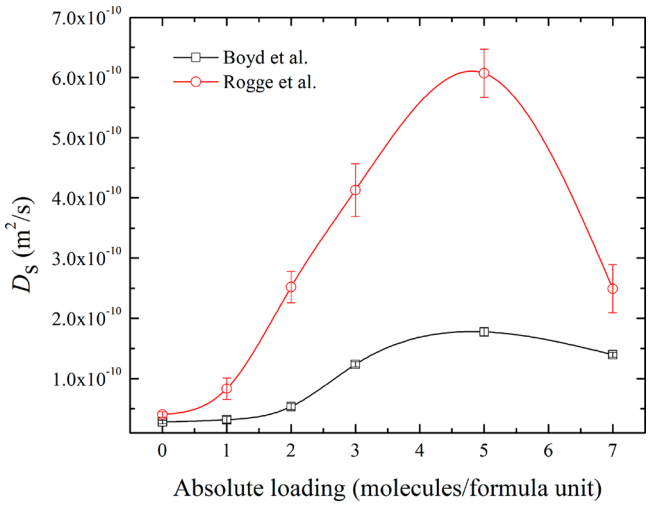

Figure 5. Effect of loading on the diffusion coefficient for the Boyd et al.[43] and Rogge et al.[44] potentials.

two potentials; diffusivity increases with increasing coverage, until the pores are filled with a liquidlike density of acetone, where the diffusivity decreases. This result is in qualitative agreement with reported literature results for CO_2 and CH_4 in dehydroxylated UiO-66, where diffusivity increased at low loading and decreased approaching saturation.[30] Diffusion coefficients are included in Table 3.

We note that differences in the estimated errors for the diffusion coefficients in Table 3 are a result of using a different numbers of independent runs. We used 50 for the Boyd et al. potential, 25 for the Rogge et al. potential, and 10 for the TraPPE/Rogge et al. potential. Hence, the errors for the latter potential are much larger than the others but are still sufficiently small to distinguish the values from the other potentials. Use of a smaller number of independent simulations was for the sake of computational efficiency.

We note that the quantitative values of diffusion coefficients from the Boyd et al. and Rogge et al. potentials are not in agreement within the estimated errors of the simulations, with the latter potential giving larger diffusivities (Table 3). After observing these differences, we carefully examined the structures of UiO-66 predicted by these two potentials and found that the Boyd et al. potential gives a relaxed structure of

https://dx.doi.org/10.1021/acs.jpcc.0c07040
J. Phys. Chem. C 2020, 124, 28469−28478

Table 3. Diffusion as a Function of Loading for Acetone in (a) Boyd et al. Flexible UiO-66,[43] (b) Rogge et al. Flexible UiO-66,[44] and (c) TraPPE/Rogge et al. UiO-66 at 325 K[a]

N (molecules/cell)	(a) D_s (m^2/s)	(b) D_s (m^2/s)	(c) D_s (m^2/s)
0	$2.80(30) \times 10^{-11}$	$4.02(48) \times 10^{-11}$	$4.88(150) \times 10^{-12}$
1	$3.18(54) \times 10^{-11}$	$8.33(180) \times 10^{-11}$	$7.67(280) \times 10^{-12}$
2	$5.35(50) \times 10^{-11}$	$2.52(26) \times 10^{-10}$	$1.92(53) \times 10^{-11}$
3	$1.24(4) \times 10^{-10}$	$4.13(44) \times 10^{-10}$	$4.40(190) \times 10^{-11}$
5	$1.78(7) \times 10^{-10}$	$6.07(40) \times 10^{-10}$	$1.44(48) \times 10^{-10}$
7	$1.40(4) \times 10^{-10}$	$2.49(40) \times 10^{-10}$	$8.47(100) \times 10^{-11}$

[a]Uncertainties in the least significant digits are given in parentheses (see Table 1).

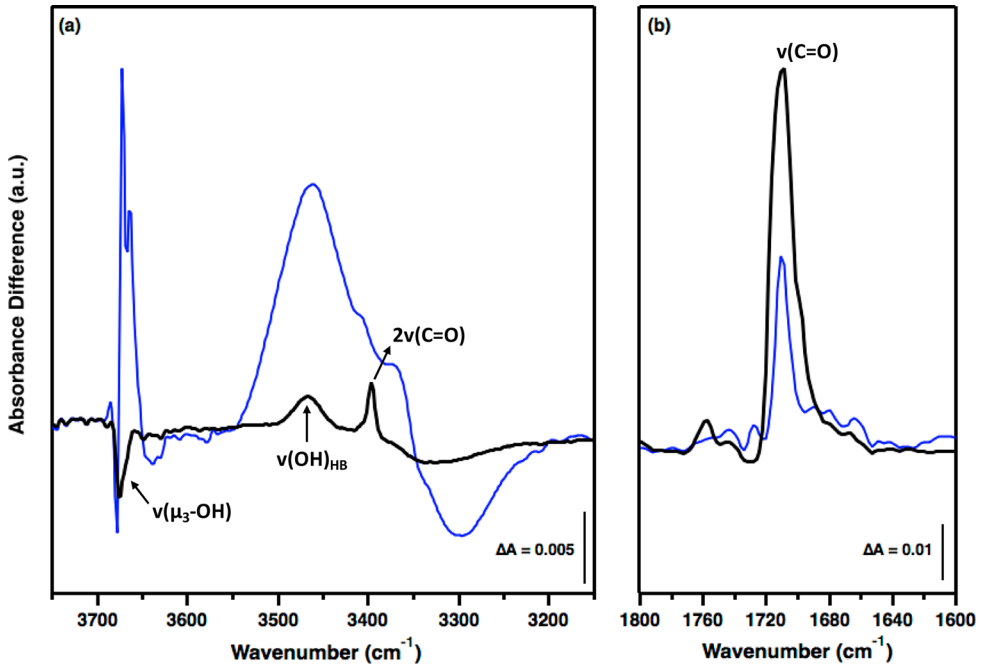

Figure 6. IR difference spectra following acetone exposure at 100 K (black) highlighting (a) the formation of hydrogen-bonded OH species, $\upsilon(OH)_{HB}$, from interaction of the μ_3-OH groups, $\upsilon(\mu_3\text{-OH})$, and (b) the carbonyl of acetone. Evolution of $\upsilon(OH)_{HB}$ is monitored as the sample temperature is increased to 240 K (blue). IR difference spectra were generated by using the clean MOF at 100 K as the reference.

the SBU that is unphysical, with some μ_3-O atoms relaxing toward the center of the SBU and overlapping. This can be seen from Figure S8 and a movie of the relaxation (just showing the SBU) also in the Supporting Information. This is surprising because the Boyd et al. potential was reported to give good values of the bulk modulus (UFF in Table 2 of Boyd et al.[43]). We therefore assume that the diffusivities computed from the Rogge et al. potential are more accurate than those computed from the Boyd et al. potential.

Up to this point, we have used published classical potentials to compute diffusivities of acetone in UiO-66. The Lennard-Jones terms for these potentials, which govern the van der Waals interactions between the acetone and framework, were taken from UFF.[61] However, we have not examined whether these classical potentials correctly account for hydrogen bonding between the μ_3-OH and acetone. Before doing this, it is important to establish whether or not acetone−framework hydrogen bonding is important.

To this end, we have performed temperature-programmed infrared (TP-IR) experiments to characterize the interactions between acetone and UiO-66. Acetone was dosed (1000 L) at 100 K on the low-defect UiO-66 sample under UHV conditions, resulting in the formation of a film of solid acetone on the external surfaces of the MOF crystallite. It is apparent from the IR difference spectra shown in Figure 6 that upon adsorption at 100 K (black curve) a small fraction of the acetone directly interacts with the μ_3-OH groups on the node (negative, $\upsilon(OH)_{free}$ at 3677 cm^{-1}) and forms hydrogen-bonding interactions with the acetone carbonyl (positive, $\upsilon(OH)_{HB}$ at 3467 cm^{-1}). Initially at 100 K (black), acetone condenses on the external MOF surface, where only a small percentage of μ_3-OH groups reside. The sample was then ramped to 240 K, resulting in a substantial growth of $\upsilon(OH)_{HB}$ (Figure 6a, blue) providing evidence that acetone has diffused into the MOF pores where majority of the μ_3-OH groups are located.

The acetone carbonyl $\upsilon(C{=}O)$ feature at 1709 cm^{-1} (Figure 6b) provides a direct spectroscopic measure for the amount of adsorbed acetone[62] and reveals an initial loss in intensity when the sample temperature increased from 100 K (Figure 6b black) to 240 K (Figure 6b blue), likely the result of acetone desorbing from the multilayer film on the external MOF surface. However, it should be noted that at this temperature (240 K) the majority of the acetone has diffused into the MOF pores, evidenced by the large increase in $\upsilon(OH)_{HB}$.

https://dx.doi.org/10.1021/acs.jpcc.0c07040
J. Phys. Chem. C 2020, 124, 28469−28478

In summary, the TP-IR results provide strong direct evidence of formation of hydrogen bonding between acetone and the framework μ_3-OH groups.

As a second method for assessing the importance of acetone−framework hydrogen bonding, we have performed DFT calculations to identify the most favorable binding sites for acetone in UiO-66. The binding energies and relative energies of acetone in each of the three types of pores of UiO-66 (tetrahedral with μ_3-OH, tetrahedral with μ_3-O, and octahedral) have been computed. The lowest energy configuration we have identified is for acetone forming a hydrogen bond with the μ_3-OH group, as shown in Figure S9. The most favorable configurations in the tetrahedral μ_3-O and octahedral pores are given in Figures S10 and S11, respectively. The binding energy of acetone in the tetrahedral μ_3-OH pore is predicted to be about 29 and 39 kJ/mol more favorable than in the tetrahedral μ_3-O and octahedral pores, respectively. Binding energy values are summarized in Table S1. The DFT predicted binding energy relative to gas phase acetone is −87.5 kJ/mol. This value is in rough agreement with TPD-MS calculated binding energies shown for a range of different prefactors in Table S2. The TPD-MS results are in general agreement for acetone adsorption in other porous materials.[63]

We have calculated binding energies of acetone in the different pores of UiO-66 using the Rogge et al. potential and the standard UFF Lennard-Jones terms and our calculated charges. We found, however, that this potential does not account for hydrogen bonding, as can be seen from the difference in binding energies of acetone in the tetrahedral μ_3-OH and μ_3-O pores of only 5.5 kJ/mol (Table S3). Examination of the potentials identified the problem as being the Lennard-Jones diameter parameter used for hydrogen in the μ_3-OH group; this parameter effectively prohibits the oxygen atom of acetone from getting closer than about 0.28 nm to the H atom of μ_3-OH, whereas hydrogen bonds are typically <0.2 nm. Indeed, our DFT calculations give a hydrogen bond distance of about 0.18 nm for acetone μ_3-OH. We have therefore developed a modified potential for the adsorbate−framework cross-interactions by replacing the O and H Lennard-Jones parameters for the μ_3-OH cross-interactions with adsorbate molecules with the O and H parameters used for the TraPPE isopropanol potential,[64] namely, $\sigma_H = \varepsilon_H = 0$, $\sigma_O = 0.302$ nm, and $\varepsilon_O = 93$ K. The binding energies for acetone in the pores calculated using these cross-parameters are in very good agreement with our DFT calculations, with the binding energy of acetone in the tetrahedral μ_3-OH pore about 23 and 40 kJ/mol more favorable than in the tetrahedral μ_3-O and octahedral pores, respectively (see Table S4). The absolute binding energy of acetone in the tetrahedral μ_3-OH pore is −75.4 kJ/mol, which is about 12 kJ/mol more weakly bound than predicted by DFT and in excellent agreement with the TPD-MS results (Table S2).

We have used this TraPPE/Rogge et al. potential to compute the diffusivities of acetone at zero loading as a function of temperature. The calculated values (Table 1) are roughly an order of magnitude smaller than the corresponding values for the Rogge et al. potential, which indicates that adsorbate−framework hydrogen bonding has a profound impact on the diffusivity. The calculated barrier to diffusion computed from the Arrhenius equation from the TraPPE/Rogge et al. simulations (Figure 2) is 27.2 kJ/mol, which is 10.7 kJ/mol higher than without hydrogen bonding.

The diffusivities of acetone for the TraPPE/Rogge et al. potential as a function of loading are given in Table 3. Comparison with the diffusivities from the Rogge et al. potential reveal that hydrogen bonding decreases the diffusivity by about 1 order of magnitude at low loading and about a factor of 3 at high loading. A plot of the loading dependent diffusivities for the Rogge et al. and TraPPE/Rogge et al. potentials is given in Figure 7. We see from this figure that the

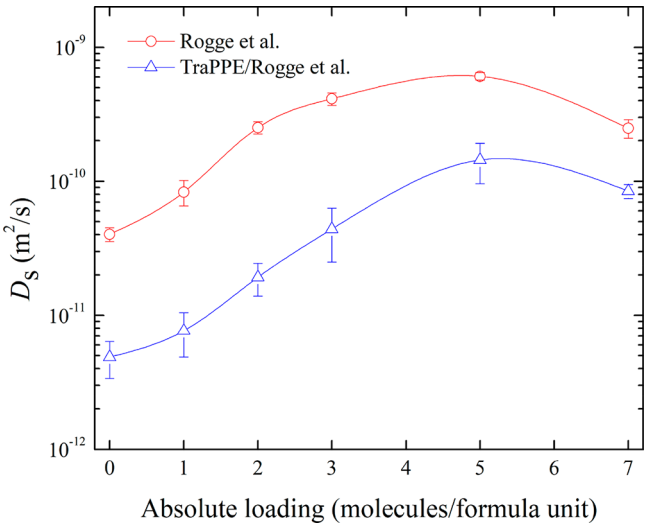

Figure 7. Loading-dependent diffusivities for acetone in UiO-66 computed from the Rogge et al. potential and the TraPPE/Rogge et al. potential.

diffusivity is qualitatively the same with and without hydrogen bonding but shifted to much lower values. From this we conclude that accounting for adsorbate−framework hydrogen bonding is necessary to get a quantitative picture of diffusion but is not required if one is only interested in the qualitative behavior.

We have computed the fraction of acetone molecules that are hydrogen bonded to μ_3-OH groups as a function of loading (averaged over the length of the simulation) and also the fraction of μ_3-OH groups that are hydrogen bonded to acetone as a function of loading, shown in Figure 8. As expected, the fraction of acetone molecules hydrogen bonded decreases with increased loading and the fraction of μ_3-OH groups hydrogen bonded increases with loading. Even at high loading, the fraction of acetone molecules hydrogen bonded is surprisingly high. The fraction of μ_3-OH groups hydrogen bonded is always <50%, which indicates that steric hindrance likely prevents more than two acetone molecules in a single pore from forming hydrogen bonds to the μ_3-OH groups on the SBUs.

CONCLUSIONS

We have shown that a flexible potential model is necessary to obtain qualitatively correct diffusivities of acetone in UiO-66 and that the mechanism of diffusion involves the BDC linkers dynamically accommodating acetone as it moves through the triangular window of the pore. Diffusivities initially increase with loading at low coverage and then decrease as saturation is approached. Hydrogen bonding between acetone and the framework μ_3-OH groups has been shown to be important from both experimental (TP-IR) and theoretical (DFT) studies. However, the potentials from the literature we have

https://dx.doi.org/10.1021/acs.jpcc.0c07040
J. Phys. Chem. C 2020, 124, 28469−28478

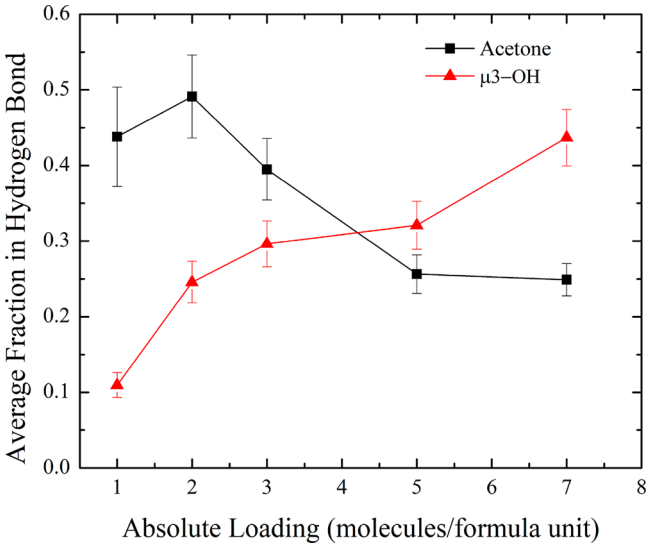

Figure 8. Fraction of acetone hydrogen bonded to framework μ_3-OH groups and the fraction of framework μ_3-OH groups that are hydrogen bonded to the node as a function of acetone loading in UiO-66 by using the TraPPE/Rogge et al. potential.

tested do not allow for an accurate accounting of hydrogen bonding. We have constructed a modified potential that allows for hydrogen bond interactions between adsorbate molecules and the framework. Diffusivities computed with hydrogen bonding are roughly an order of magnitude smaller than when hydrogen bonding is ignored.

■ ASSOCIATED CONTENT

Supporting Information

The Supporting Information is available free of charge at https://pubs.acs.org/doi/10.1021/acs.jpcc.0c07040.

Force field details, grand canonical Monte Carlo simulation details and results, materials synthesis and characterization details, ligand defect estimates, experimental characterization methods, density functional theory simulation details, TP IR details, TPD-MS details and results (PDF)
LAMMPS input files (ZIP)
Movie S1 (MPG)
Movie S2 (MPG)
Movie S3 (MPG)

■ AUTHOR INFORMATION

Corresponding Author

J. Karl Johnson − *Department of Chemical and Petroleum Engineering, University of Pittsburgh, Pittsburgh, Pennsylvania 15261, United States;* orcid.org/0000-0002-3608-8003; Email: karlj@pitt.edu

Authors

Jacob J. Wardzala − *Department of Chemical and Petroleum Engineering, University of Pittsburgh, Pittsburgh, Pennsylvania 15261, United States*

Jonathan P. Ruffley − *Department of Chemical and Petroleum Engineering, University of Pittsburgh, Pittsburgh, Pennsylvania 15261, United States*

Isabella Goodenough − *Department of Chemistry, Temple University, Philadelphia, Pennsylvania 19122, United States;* orcid.org/0000-0001-8581-4473

Allie M. Schmidt − *Department of Chemical and Petroleum Engineering, University of Pittsburgh, Pittsburgh, Pennsylvania 15261, United States*

Priyanka B. Shukla − *Department of Chemical and Petroleum Engineering, University of Pittsburgh, Pittsburgh, Pennsylvania 15261, United States*

Xin Wei − *Department of Chemical and Petroleum Engineering, University of Pittsburgh, Pittsburgh, Pennsylvania 15261, United States*

Abhishek Bagusetty − *Department of Chemical and Petroleum Engineering, University of Pittsburgh, Pittsburgh, Pennsylvania 15261, United States*

Mattheus De Souza − *Department of Chemistry, University of Pittsburgh, Pittsburgh, Pennsylvania 15261, United States;* orcid.org/0000-0002-2057-3610

Prasenjit Das − *Department of Chemistry, University of Pittsburgh, Pittsburgh, Pennsylvania 15261, United States*

Dorian J. Thompson − *Department of Chemical and Petroleum Engineering, University of Pittsburgh, Pittsburgh, Pennsylvania 15261, United States*

Christopher J. Karwacki − *U.S. Army Combat Capabilities Development Command Chemical Biological Center, Aberdeen, Maryland 21010, United States*

Christopher E. Wilmer − *Department of Chemical and Petroleum Engineering, University of Pittsburgh, Pittsburgh, Pennsylvania 15261, United States; Department of Electrical and Computer Engineering, University of Pittsburgh, Pittsburgh, Pennsylvania 15261, United States*

Eric Borguet − *Department of Chemistry, Temple University, Philadelphia, Pennsylvania 19122, United States;* orcid.org/0000-0003-0593-952X

Nathaniel L. Rosi − *Department of Chemical and Petroleum Engineering, University of Pittsburgh, Pittsburgh, Pennsylvania 15261, United States; Department of Chemistry, University of Pittsburgh, Pittsburgh, Pennsylvania 15261, United States;* orcid.org/0000-0001-8025-8906

Complete contact information is available at: https://pubs.acs.org/10.1021/acs.jpcc.0c07040

Notes

The authors declare no competing financial interest.

■ ACKNOWLEDGMENTS

This research was sponsored by the Army Research Office and was accomplished under Cooperative Agreement W911NF-19-2-0187. Partial support for this work was provided by the Defense Threat Reduction Agency (DTRA) (Grant HDTRA1-16-1-0044). Computations were performed at the University of Pittsburgh's Center for Research Computing, the Pittsburgh Supercomputer Center, through a grant from the Extreme Science and Engineering Discovery Environment (XSEDE), which is supported by National Science Foundation Grant ACI-1548562 under Allocation TG-DMR110091, and the U.S. Army Engineer Research and Development Center DoD Supercomputer Resource Center. We thank Liangliang Huang and Shanshan Wang for helpful discussions.

■ REFERENCES

(1) Furukawa, H.; Cordova, K. E.; O'Keeffe, M.; Yaghi, O. M. The Chemistry and Applications of Metal-Organic Frameworks. *Science* **2013**, *341*, 1230444−1230444.
(2) Zhou, H.-C.; Long, J. R.; Yaghi, O. M. Introduction to Metal−Organic Frameworks. *Chem. Rev.* **2012**, *112*, 673−674.

(3) Ahmad, M. Z.; Peters, T. A.; Konnertz, N. M.; Visser, T.; Téllez, C.; Coronas, J.; Fila, V.; de Vos, W. M.; Benes, N. E. High-Pressure CO_2/CH_4 Separation of Zr-MOFs Based Mixed Matrix Membranes. *Sep. Purif. Technol.* **2020**, *230*, 115858.
(4) Bae, T.-H.; Lee, J. S.; Qiu, W.; Koros, W. J.; Jones, C. W.; Nair, S. A High-Performance Gas-Separation Membrane Containing Submicrometer-Sized Metal-Organic Framework Crystals. *Angew. Chem., Int. Ed.* **2010**, *49*, 9863−9866.
(5) Mohamed, M. H.; Yang, Y.; Li, L.; Zhang, S.; Ruffley, J. P.; Jarvi, A. G.; Saxena, S.; Veser, G.; Johnson, J. K.; Rosi, N. L. Designing Open Metal Sites in Metal−Organic Frameworks for Paraffin/Olefin Separations. *J. Am. Chem. Soc.* **2019**, *141*, 13003−13007.
(6) Xie, Z.; Li, T.; Rosi, N. L.; Carreon, M. A. Alumina-Supported Cobalt−Adeninate MOF Membranes for CO_2/CH_4 Separation. *J. Mater. Chem. A* **2014**, *2*, 1239−1241.
(7) Ruffley, J. P.; Goodenough, I.; Luo, T.-Y.; Richard, M.; Borguet, E.; Rosi, N. L.; Johnson, J. K. Design, Synthesis, and Characterization of Metal−Organic Frameworks for Enhanced Sorption of Chemical Warfare Agent Simulants. *J. Phys. Chem. C* **2019**, *123*, 19748−19758.
(8) Nemati Vesali Azar, A.; Keskin, S. Computational Screening of MOFs for Acetylene Separation *Front. Chem.* **2018**, .
(9) Li, L.; Zhang, S.; Ruffley, J. P.; Johnson, J. K. Energy Efficient Formaldehyde Synthesis by Direct Hydrogenation of Carbon Monoxide in Functionalized Metal−Organic Frameworks. *ACS Sustainable Chem. Eng.* **2019**, *7*, 2508−2515.
(10) Han, S.; Huang, Y.; Watanabe, T.; Nair, S.; Walton, K. S.; Sholl, D. S.; Carson Meredith, J. MOF Stability and Gas Adsorption as a Function of Exposure to Water, Humid Air, SO_2, and NO_2. *Microporous Mesoporous Mater.* **2013**, *173*, 86−91.
(11) Grant Glover, T.; Peterson, G. W.; Schindler, B. J.; Britt, D.; Yaghi, O. MOF-74 Building Unit has a Direct Impact on Toxic Gas Adsorption. *Chem. Eng. Sci.* **2011**, *66*, 163−170.
(12) Kirlikovali, K. O.; Chen, Z.; Islamoglu, T.; Hupp, J. T.; Farha, O. K. Zirconium-Based Metal−Organic Frameworks for the Catalytic Hydrolysis of Organophosphorus Nerve Agents. *ACS Appl. Mater. Interfaces* **2020**, *12*, 14702−14720.
(13) Liu, Y.; Howarth, A. J.; Vermeulen, N. A.; Moon, S.-Y.; Hupp, J. T.; Farha, O. K. Catalytic Degradation of Chemical Warfare Agents and Their Simulants by Metal-Organic Frameworks. *Coord. Chem. Rev.* **2017**, *346*, 101−111.
(14) Mondloch, J. E.; Katz, M. J.; Isley, W. C., III; Ghosh, P.; Liao, P.; Bury, W.; Wagner, G. W.; Hall, M. G.; DeCoste, J. B.; Peterson, G. W.; Snurr, R. Q.; Cramer, C. J.; Hupp, J. T.; Farha, O. K. Destruction of Chemical Warfare Agents Using Metal−Organic Frameworks. *Nat. Mater.* **2015**, *14*, 512−516.
(15) Islamoglu, T.; Chen, Z.; Wasson, M. C.; Buru, C. T.; Kirlikovali, K. O.; Afrin, U.; Mian, M. R.; Farha, O. K. Metal−Organic Frameworks Against Toxic Chemicals. *Chem. Rev.* **2020**, *120*, 8130.
(16) Son, F. A.; Wasson, M. C.; Islamoglu, T.; Chen, Z.; Gong, X.; Hanna, S. L.; Lyu, J.; Wang, X.; Idrees, K. B.; Mahle, J. J.; et al. Uncovering the Role of Metal−Organic Framework Topology on the Capture and Reactivity of Chemical Warfare Agents. *Chem. Mater.* **2020**, *32*, 4609−4617.
(17) Valenzano, L.; Civalleri, B.; Chavan, S.; Bordiga, S.; Nilsen, M. H.; Jakobsen, S.; Lillerud, K. P.; Lamberti, C. Disclosing the Complex Structure of UiO-66 Metal Organic Framework: A Synergic Combination of Experiment and Theory. *Chem. Mater.* **2011**, *23*, 1700−1718.
(18) Shearer, G. C.; Forselv, S.; Chavan, S.; Bordiga, S.; Mathisen, K.; Bjørgen, M.; Svelle, S.; Lillerud, K. P. In Situ Infrared Spectroscopic and Gravimetric Characterisation of the Solvent Removal and Dehydroxylation of the Metal Organic Frameworks UiO-66 and UiO-67. *Top. Catal.* **2013**, *56*, 770−782.
(19) Agrawal, M.; Boulfelfel, S. E.; Sava Gallis, D. F.; Greathouse, J. A.; Sholl, D. S. Determining Diffusion Coefficients of Chemical Warfare Agents in Metal−Organic Frameworks. *J. Phys. Chem. Lett.* **2019**, *10*, 7823−7830.
(20) Ramsahye, N. A.; Maurin, G. Modeling of Diffusion in MOFs. In *Modelling and Simulation in the Science of Micro- and Meso-Porous Materials*, Catlow, C. R. A.; van Santen, R. A., Eds., Elsevier, **2017**; pp 63−97.
(21) Skoulidas, A. I. Molecular Dynamics Simulations of Gas Diffusion in Metal−Organic Frameworks: Argon in CuBTC. *J. Am. Chem. Soc.* **2004**, *126*, 1356−1357.
(22) Parkes, M. V.; Demir, H.; Teich-McGoldrick, S. L.; Sholl, D. S.; Greathouse, J. A.; Allendorf, M. D. Molecular dynamics simulation of framework flexibility effects on noble gas diffusion in HKUST-1 and ZIF-8. *Microporous Mesoporous Mater.* **2014**, *194*, 190−199.
(23) Liu, B.; Yang, Q.; Xue, C.; Zhong, C.; Smit, B. Molecular Simulation of Hydrogen Diffusion in Interpenetrated Metal−Organic Frameworks. *Phys. Chem. Chem. Phys.* **2008**, *10*, 3244.
(24) Liu, B.; Sun, C.; Chen, G. Molecular Simulation Studies of Separation of CH_4/H_2 Mixture in Metal-Organic Frameworks with Interpenetration and Mixed-Ligand. *Chem. Eng. Sci.* **2011**, *66*, 3012−3019.
(25) Keskin, S. Gas Adsorption and Diffusion in a Highly CO_2 Selective Metal−Organic Framework: Molecular Simulations. *Mol. Simul.* **2013**, *39*, 14−24.
(26) Farzi, N.; Salehi, N.; Mahboubi, A. Molecular Dynamics Simulation of Acetylene Diffusion in MOF-508a and MOF-508b. *Microporous Mesoporous Mater.* **2017**, *248*, 246−255.
(27) Cabrales-Navarro, F. A.; Gómez-Ballesteros, J. L.; Balbuena, P. B. Molecular Dynamics Simulations of Metal-Organic Frameworks as Membranes for Gas Mixtures Separation. *J. Membr. Sci.* **2013**, *428*, 241−250.
(28) Borah, B.; Zhang, H.; Snurr, R. Q. Diffusion of Methane and Other Alkanes in Metal-Organic Frameworks for Natural Gas Storage. *Chem. Eng. Sci.* **2015**, *124*, 135−143.
(29) Bigdeli, A.; Khorasheh, F.; Tourani, S.; Khoshgard, A.; Bidaroni, H. H. Molecular Simulation Study of the Adsorption and Diffusion Properties of Terephthalic Acid in Various Metal Organic Frameworks. *J. Inorg. Organomet. Polym. Mater.* **2020**, *30*, 1643−1652.
(30) Yang, Q.; Jobic, H.; Salles, F.; Kolokolov, D.; Guillerm, V.; Serre, C.; Maurin, G. Probing the Dynamics of CO_2 and CH_4 within the Porous Zirconium Terephthalate UiO-66(Zr): A Synergic Combination of Neutron Scattering Measurements and Molecular Simulations. *Chem. - Eur. J.* **2011**, *17*, 8882−8889.
(31) Vargas, L. E.; Snurr, R. Q. Heterogeneous Diffusion of Alkanes in the Hierarchical Metal−Organic Framework NU-1000. *Langmuir* **2015**, *31*, 10056−10065.
(32) Skoulidas, A. I.; Sholl, D. S. Self-Diffusion and Transport Diffusion of Light Gases in Metal-Organic Framework Materials Assessed Using Molecular Dynamics Simulations. *J. Phys. Chem. B* **2005**, *109*, 15760−15768.
(33) Amirjalayer, S.; Tafipolsky, M.; Schmid, R. Molecular Dynamics Simulation of Benzene Diffusion in MOF-5: Importance of Lattice Dynamics. *Angew. Chem., Int. Ed.* **2007**, *46*, 463−466.
(34) Koizumi, K.; Nobusada, K.; Boero, M. Hydrogen Storage Mechanism and Diffusion in Metal−Organic Frameworks. *Phys. Chem. Chem. Phys.* **2019**, *21*, 7756−7764.
(35) Liu, J.; Rankin, R. B.; Karl Johnson, J. The Importance of Charge−Quadrupole Interactions for H_2 Adsorption and Diffusion in CuBTC. *Mol. Simul.* **2009**, *35*, 60−69.
(36) Liu, J.; Lee, J. Y.; Pan, L.; Obermyer, R. T.; Simizu, S.; Zande, B.; Li, J.; Sankar, S. G.; Johnson, J. K. Adsorption and Diffusion of Hydrogen in a New Metal−Organic Framework Material: [Zn(bdc)-(ted)0.5]. *J. Phys. Chem. C* **2008**, *112*, 2911−2917.
(37) Keskin, S.; Liu, J.; Johnson, J. K.; Sholl, D. S. Atomically Detailed Models of Gas Mixture Diffusion Through CuBTC Membranes. *Microporous Mesoporous Mater.* **2009**, *125*, 101−106.
(38) Keskin, S.; Liu, J.; Johnson, J. K.; Sholl, D. S. Testing the Accuracy of Correlations for Multicomponent Mass Transport of Adsorbed Gases in Metal−Organic Frameworks: Diffusion of H_2/CH_4 Mixtures in CuBTC. *Langmuir* **2008**, *24*, 8254−8261.
(39) Skoulidas, A. I.; Sholl, D. S. Molecular Dynamics Simulations of Self-Diffusivities, Corrected Diffusivities, and Transport Diffusivities of Light Gases in Four Silica Zeolites To Assess Influences of Pore Shape and Connectivity. *J. Phys. Chem. A* **2003**, *107*, 10132−10141.

https://dx.doi.org/10.1021/acs.jpcc.0c07040
J. Phys. Chem. C 2020, 124, 28469−28478

(40) Grissom, T. G.; Sharp, C. H.; Usov, P. M.; Troya, D.; Morris, A. J.; Morris, J. R. Benzene, Toluene, and Xylene Transport through UiO-66: Diffusion Rates, Energetics, and the Role of Hydrogen Bonding. *J. Phys. Chem. C* **2018**, *122*, 16060−16069.
(41) Sharp, C. H.; Abelard, J.; Plonka, A. M.; Guo, W.; Hill, C. L.; Morris, J. R. Alkane−OH Hydrogen Bond Formation and Diffusion Energetics of n-Butane within UiO-66. *J. Phys. Chem. C* **2017**, *121*, 8902−8906.
(42) Plimpton, S. Fast Parallel Algorithms for Short-Range Molecular Dynamics. *J. Comput. Phys.* **1995**, *117*, 1−19.
(43) Boyd, P. G.; Moosavi, S. M.; Witman, M.; Smit, B. Force-Field Prediction of Materials Properties in Metal-Organic Frameworks. *J. Phys. Chem. Lett.* **2017**, *8*, 357−363.
(44) Rogge, S. M. J.; Wieme, J.; Vanduyfhuys, L.; Vandenbrande, S.; Maurin, G.; Verstraelen, T.; Waroquier, M.; Van Speybroeck, V. Thermodynamic Insight in the High-Pressure Behavior of UiO-66: Effect of Linker Defects and Linker Expansion. *Chem. Mater.* **2016**, *28*, 5721−5732.
(45) Manz, T. A.; Limas, N. G. Introducing DDEC6 Atomic Population Analysis: Part 1. Charge Partitioning Theory and Methodology. *RSC Adv.* **2016**, *6*, 47771−47801.
(46) Manz, T. A. Introducing DDEC6 Atomic Population Analysis: Part 3. Comprehensive Method to Compute Bond Orders. *RSC Adv.* **2017**, *7*, 45552−45581.
(47) Limas, N. G.; Manz, T. A. Introducing DDEC6 Atomic Population Analysis: Part 4. Efficient Parallel Computation of Net Atomic Charges, Atomic Spin Moments, Bond Orders, and More. *RSC Adv.* **2018**, *8*, 2678−2707.
(48) Limas, N. G.; Manz, T. A. Introducing DDEC6 Atomic Population Analysis: Part 2. Computed Results for a Wide Range of Periodic and Nonperiodic Materials. *RSC Adv.* **2016**, *6*, 45727−45747.
(49) Stubbs, J. M.; Potoff, J. J.; Siepmann, J. I. Transferable Potentials for Phase Equilibria. 6. United-Atom Description for Ethers, Glycols, Ketones, and Aldehydes. *J. Phys. Chem. B* **2004**, *108*, 17596−17605.
(50) Morales, J. J.; Nuevo, M. J. Path Integral Molecular Dynamics Methods: Application to Neon. *J. Comput. Chem.* **1995**, *16*, 105−112.
(51) Nosé, S. A Unified Formulation of the Constant Temperature Molecular Dynamics Methods. *J. Chem. Phys.* **1984**, *81*, 511−519.
(52) Hoover, W. G. Canonical Dynamics: Equilibrium Phase-Space Distributions. *Phys. Rev. A: At., Mol., Opt. Phys.* **1985**, *31*, 1695−1697.
(53) Agrawal, M.; Sava Gallis, D. F.; Greathouse, J. A.; Sholl, D. S. How Useful Are Common Simulants of Chemical Warfare Agents at Predicting Adsorption Behavior? *J. Phys. Chem. C* **2018**, *122*, 26061−26069.
(54) Fiorin, G.; Klein, M. L.; Hénin, J. Using Collective Variables to Drive Molecular Dynamics Simulations. *Mol. Phys.* **2013**, *111*, 3345−3362.
(55) Grossfield, A. *WHAM: The Weighted Histogram Analysis Method*, 2.0.10.1.
(56) Shearer, G. C.; Chavan, S.; Ethiraj, J.; Vitillo, J. G.; Svelle, S.; Olsbye, U.; Lamberti, C.; Bordiga, S.; Lillerud, K. P. Tuned to Perfection: Ironing Out the Defects in Metal−Organic Framework UiO-66. *Chem. Mater.* **2014**, *26*, 4068−4071.
(57) Kwon, S.; Vidic, R.; Borguet, E. The Effect of Surface Chemical Functional Groups on the Adsorption and Desorption of a Polar Molecule, Acetone, from a Model Carbonaceous Surface, Graphite. *Surf. Sci.* **2003**, *522*, 17−26.
(58) Breck, D. W. *Zeolite Molecular Sieves: Structure, Chemistry, and Use*; Wiley: New York, 1973; p ix, 771 pp.
(59) Cavka, J. H.; Jakobsen, S.; Olsbye, U.; Guillou, N.; Lamberti, C.; Bordiga, S.; Lillerud, K. P. A New Zirconium Inorganic Building Brick Forming Metal Organic Frameworks with Exceptional Stability. *J. Am. Chem. Soc.* **2008**, *130*, 13850−13851.
(60) Ramsahye, N. A.; Gao, J.; Jobic, H.; Llewellyn, P. L.; Yang, Q.; Wiersum, A. D.; Koza, M. M.; Guillerm, V.; Serre, C.; Zhong, C. L.; et al. Adsorption and Diffusion of Light Hydrocarbons in UiO-66(Zr): A Combination of Experimental and Modeling Tools. *J. Phys. Chem. C* **2014**, *118*, 27470−27482.
(61) Rappe, A. K.; Casewit, C. J.; Colwell, K. S.; Goddard, W. A.; Skiff, W. M. UFF, a Full Periodic Table Force Field for Molecular Mechanics and Molecular Dynamics Simulations. *J. Am. Chem. Soc.* **1992**, *114*, 10024−10035.
(62) Kazachkin, D. V.; Nishimura, Y.; Witek, H. A.; Irle, S.; Borguet, E. Dramatic Reduction of IR Vibrational Cross Sections of Molecules Encapsulated in Carbon Nanotubes. *J. Am. Chem. Soc.* **2011**, *133*, 8191−8198.
(63) Kazachkin, D.; Nishimura, Y.; Irle, S.; Morokuma, K.; Vidic, R. D.; Borguet, E. Interaction of Acetone with Single Wall Carbon Nanotubes at Cryogenic Temperatures: A Combined Temperature Programmed Desorption and Theoretical Study. *Langmuir* **2008**, *24*, 7848−7856.
(64) Chen, B.; Potoff, J. J.; Siepmann, J. I. Monte Carlo Calculations for Alcohols and Their Mixtures with Alkanes. Transferable Potentials for Phase Equilibria. 5. United-Atom Description of Primary, Secondary, and Tertiary Alcohols. *J. Phys. Chem. B* **2001**, *105*, 3093−3104.

https://dx.doi.org/10.1021/acs.jpcc.0c07040
J. Phys. Chem. C 2020, 124, 28469−28478